Earth's Future

RESEARCH ARTICLE
10.1029/2022EF003225

High-Tide Flooding Along the China Coastline: Past and Future

S. Li[1], T. Wahl[2], J. Fang[3], L. Liu[1], and T. Jiang[4]

[1]State Key Laboratory of Geodesy and Earth's Dynamics, Innovation Academy for Precision Measurement Science and Technology, Chinese Academy of Sciences, Wuhan, China, [2]Department of Civil, Environmental and Construction Engineering and National Center for Integrated Coastal Research, University of Central Florida, Orlando, FL, USA, [3]Zhejiang Provincial Key Laboratory of Urban Wetlands and Regional Change, School of Information Science and Technology, Institute of Remote Sensing and Earth Sciences, Hangzhou Normal University, Hangzhou, China, [4]Jiangsu Ocean University, Lianyungang, China

Key Points:

- The frequency of High-tide flooding (HTF) along China coastline has increased, with a doubling time of 11.5–37.4 years in Xiamen
- Cumulative loss ratios of HTF are higher than those of extreme flooding at several locations
- China will experience more HTF days under all warming scenarios, with more rapid increases in the 2030s and 2050s

Supporting Information:

Supporting Information may be found in the online version of this article.

Correspondence to:

S. Li and L. Liu,
s.li@knights.ucf.edu;
llt@asch.whigg.ac.cn

Citation:

Li, S., Wahl, T., Fang, J., Liu, L., & Jiang, T. (2023). High-tide flooding along the China coastline: Past and future. *Earth's Future*, *11*, e2022EF003225. https://doi.org/10.1029/2022EF003225

Received 22 SEP 2022
Accepted 14 MAR 2023

Author Contributions:

Conceptualization: S. Li
Funding acquisition: L. Liu
Software: S. Li
Writing – original draft: S. Li
Writing – review & editing: T. Wahl

Abstract Coastal flooding has become a major issue for low-lying coastal cities in China, and a lot of research has focused on assessing flood risk from storms and associated extreme sea levels. High-tide flooding (HTF), however, which leads to minor inundation and occurs more frequently as sea level continues to rise has not been assessed comprehensively. Here, we analyze HTF along the China coastline using tide gauge records. We show that the frequency of HTF has increased (Xiamen doubled HTF frequency every 11.5–37.4 years, with the median being 17.5 years). As a result, the cumulative loss ratios of HTF are higher than those of major (or extreme) flooding events in several locations. To gain insights into the processes driving HTF changes, we decompose still water levels that occurred during HTF into five components, including non-linear trend, interannual to decadal mean sea level (MSL) variability, seasonal MSL cycle, tidal anomaly, and nontidal residuals. It is evident that due to sea-level rise (SLR) fewer components need to combine to raise the water levels above HTF thresholds. We show that the South China Sea coast already experiences HTF purely driven by high spring tides, and will also see the fastest future increase in the number of tide-only HTF events. In general, China will experience more HTF days under all warming scenarios as SLRs. This long-term trend will be modulated by the nodal cycle of ocean tides leading to more rapid increases in HTF in the 2030s and 2050s.

Plain Language Summary High-tide flooding (HTF), which usually occurs during high tides in coastal areas, is one of the most apparent consequences of sea-level rise (SLR). Analyses of HTF in the past and future have been carried out for the United States, Australia, and Europe, but no comprehensive analysis exists for the coast of China. Here, we analyze HTF along the China coast based on available sea level records. We find, for example, that the frequency of HTF has increased and doubled every 17.7 years. High tidal levels alone will lead to more HTF days due to SLR along the South China Sea coast. In the future, the China coast will experience more HTF days under different warming scenarios, with more rapid increases in the 2030s and 2050s due to long-term cycles in ocean tides. The analysis presented here advances our understanding of HTF along the China coastline, providing a basis for future research and adaptation planning.

1. Introduction

High-tide flooding (HTF) refers to low levels of inundation in coastal areas that usually (but not always) occur at high tide. HTF does not pose significant threats to public safety and property as the extreme storm surges do, but can cause minor property damage, road closures, public health risks, or disrupt routine activities (Cherqui et al., 2015; Hino et al., 2019; Moftakhari et al., 2018; Sweet & Park, 2014). Policymakers often pay attention to the grave consequences of extreme but rare flooding events, but the cumulative effects of recurrent HTF could be even worse (Moftakhari, AghaKouchak, et al., 2017).

Analyses of HTF in the past, present, and future have been carried out for the United States (Moftakhari et al., 2015; Sweet & Park, 2014; Taherkhani et al., 2020; Thompson et al., 2021; Vitousek et al., 2017), Australia (Hague et al., 2022; Lowe et al., 2021), and Europe (Ferrarin et al., 2022). Those studies showed that HTF frequency is increasing at a linear or exponential rate, in which sea-level rise (SLR) plays a major role. Amplified ocean tides also contribute to the increasing frequency of HTF along the US coastline (Li et al., 2021), especially in estuaries. Similar effects are likely to take place elsewhere but have yet to be quantified. The contribution of other sea-level processes (e.g., nontidal residuals [NTRs] and ocean waves) to extreme sea levels have also been

studied in Europe (Ferrarin et al., 2022), North America (Li et al., 2022; Losada et al., 2013; Serafin et al., 2017), Australia (Hague et al., 2022; Lowe et al., 2021), and globally (Melet et al., 2018; Merrifield et al., 2013; Rueda et al., 2017). The co-occurrence of two (or more) sea level components at high/moderate levels (e.g., moderate storm surges occur during the peaks of seasonal mean sea level [MSL] and tides) may lead to exceedances of higher thresholds and longer event durations, with associated adverse consequences.

Major coastal cities in the United States will experience substantial increases in HTF frequency in the coming decades (Dahl et al., 2017; Sweet et al., 2018; Thompson et al., 2021). Besides a general growth tendency in HTF frequency due to SLR, two astronomical cycles which modulate ocean tides will lead to more frequent HTF during specific periods compared to others (Ray & Foster, 2016; Thompson et al., 2021). For example, in the mid-2030s, we will likely see the onset of rapid increases in the frequency of HTF in multiple US coastal regions (Thompson et al., 2021). In addition, HTF will be more likely caused by tides alone under SLR, although it is rare in most places today (Ray & Foster, 2016; Sweet et al., 2018). By the end of this century, HTF could occur during half of the year under the intermediate-low scenario of SLR along the US east coast and Gulf coast (Burgos et al., 2018; Sweet et al., 2018).

The coast of China is also facing challenges, as climate change with associated SLR and human activities greatly increases the risk of coastal flooding. Extreme flooding events are more frequent now compared to the 1980s (Y. Chen et al., 2014; Shi et al., 2015) as a result of an increase in the magnitude of extreme sea levels due to SLR (Fang et al., 2021; J. Feng et al., 2015; Menéndez & Woodworth, 2010; Wu et al., 2017), changes in the frequency and intensity of storm surge events (Ji et al., 2021; Shi et al., 2015; K. Wang et al., 2021), increase in the occurrence of compound flooding due to extreme precipitation and storm surges (Couasnon et al., 2020; Fang et al., 2021; Xu et al., 2019), coastal subsidence from groundwater usage and other human activities (Hu et al., 2009; Tang et al., 2021; J. Wang et al., 2012), and amplification of ocean tides as a result of human interventions such as dredging (Devlin et al., 2017; J. Feng et al., 2015; Pelling et al., 2013). In addition to extreme flooding events, HTF is now more often reported by local media, for example, Beihai encountered coastal flooding during high astronomical tides in December, Xiamen in October, and Qingdao in November of 2021. However, there is currently a lack of research on HTF along the coast of China. Here we build on previous studies to assess changes in HTF in the past and future. We address the following research questions.

1. How has the HTF frequency changed along the China coastline?
2. How often is HTF caused by astronomical tides alone?
3. Are the cumulative losses from HTF bigger than those from (rare) extreme flooding events in China?
4. How will SLR change future HTF occurrences?

2. Data

Hourly water level records from 13 tidal gauge sites along the China coastline (Figure 1) are gathered from the Global Extreme Sea Level Analysis database (Haigh et al., 2022). Daily high and low tidal levels at seven sites are obtained from the Department of Water Resources of Zhejiang Province, China, which are then interpolated to hourly water levels through trigonometric interpolation (Zhang et al., 2018). Monthly and annual MSLs, as well as their datum information, are downloaded from the Permanent Service for Mean Sea Level (Holgate et al., 2013). Projections of SLR for tidal gauges along the China coastline are obtained from the National Aeronautics and Space Administration (NASA) projection tool (Fox-Kemper et al., 2021; Garner et al., 2021). Simulated water levels from 1950 to 2018 are obtained from the Copernicus Climate Change Service (C3S) Climate Data Store (CDS), which provides hourly water levels driven by storm surges, tides, and MSL derived with the Global Tide and Surge Model (GTSM) (Muis et al., 2022).

Digital elevation models (DEMs) with 30-m spatial resolution and $1° \times 1°$ tiles are obtained from the Advanced Spaceborne Thermal Emission and Reflection Radiometer Global Digital Elevation Model third version (ASTER GDEM v3) to estimate the cumulative flood losses near tidal gauges. The vertical datum of ASTER GDEM v3 is Earth Geopotential Model 96; the datum of mean dynamic ocean topography, which is employed to convert the datum of tidal observation to DEM, is Gravity Observation Combination 05s. The datum difference between mean dynamic ocean topography and DEM is computed using the International Centre for Global Earth Models (http://icgem.gfz-potsdam.de/calcpoints). A filter width of half transfer is used in a Gaussian filter when smoothing out high-frequency errors in the gravity model. We then removed MSL from water level observations, and

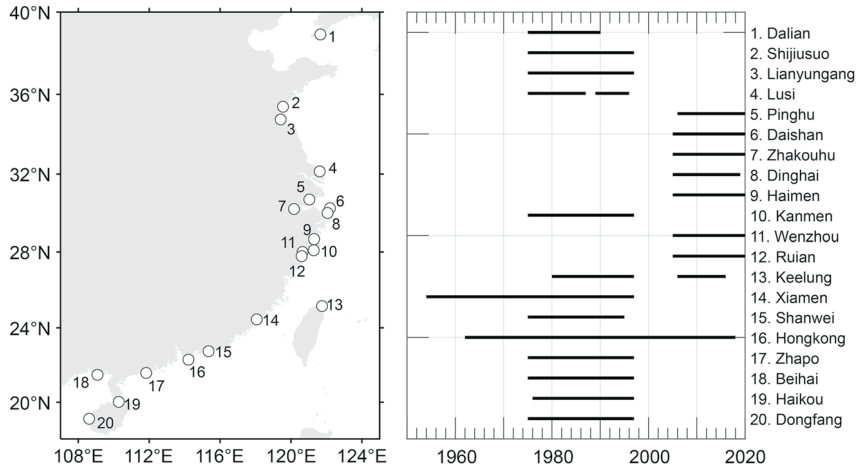

Figure 1. Data availability at 20 tidal gauge sites along the China coastline (years with >75% of hourly data are shown here). Sites from Dalian to Lusi (nos. 1–4) are located on the Yellow Sea Coast; Pinghu to Xiamen (nos. 5–14) are located on the East China Sea Coast; Shanwei to Dongfang (nos. 15–20) are located on the South China Sea Coast.

added datum difference plus mean dynamic ocean topography to the residuals. Finally, we matched the vertical datum of water level observations to DEM.

We use different thresholds for HTF (Table S1 in Supporting Information S1), which were defined by: (a) the 99th percentile of daily highest water levels (this is often considered a threshold for extreme sea levels; Haigh et al., 2010; Wahl et al., 2015); (b) we also use the 2-year return water levels as HTF threshold, which is equal to the warning level designed by the China National Standard (GB/T 22482-2008). The 2-year return water levels are obtained with non-stationary extreme value analysis for annual maximum water levels (Cheng et al., 2014; Figure S1 in Supporting Information S1); (c) the National Oceanic and Atmospheric Administration (NOAA) provides a way to infer HTF thresholds based on the diurnal range of observations (Sweet et al., 2018), namely $y = 1.04x + 0.5$, where x is the great diurnal range (in meters) and y is the HTF threshold above mean lower low water. Therefore, for each site, we have three different thresholds for HTF, which are listed in Table S1 in Supporting Information S1. The thresholds defined by the 99th percentile of daily highest water levels and 2-year return levels are close, but generally higher than interpolated thresholds using NOAA's approach. Here, we mainly focus on results from thresholds defined by the 99th percentile daily highest water levels. The results under the other two thresholds are shown in the Supporting Information for comparison.

HTF frequency refers to exceedances above the derived threshold (Sweet et al., 2018). Hence, the water levels above moderate and major flooding thresholds are also counted (Li et al., 2021; Sweet et al., 2018; Thompson et al., 2021). An exception is the analysis of cumulative losses, where events are categorized based on all three flooding stages.

3. Methods

3.1. Changes in HTF Frequency

HTF frequency refers to exceedances above the derived threshold. In our analysis, we count the number (days/year) of daily highest water levels that exceeded the HTF thresholds in each calendar year. To obtain the doubling time of HTF frequency, the HTF frequency is fitted to the exponential model ($y = ae^{bt}$). The doubling time is then estimated through

$$\frac{ae^{bt_2}}{ae^{bt_1}} = 2 \rightarrow \ln\left(e^{bt_2}\right) - \ln\left(e^{bt_1}\right) = \ln 2 \rightarrow (t_2 - t_1) = \frac{\ln 2}{b} \quad (1)$$

where $t_2 - t_1$ is the doubling time; a and b are parameters of the exponential model; t and y represent time and HTF frequency, respectively. The uncertainty in doubling time is obtained from the 95% confidence bounds of estimated b.

Due to limited data length, we make full use of available data for our analysis, that is, interpolating daily high-low data to hourly water levels. The full tidal constituents are hardly obtained when using interpolated water levels. However, we could obtain relatively accurate results for major ocean tides, whose amplitudes are only ~2% away from the accurate tidal constituents in San Francisco, CA (Table S2 in Supporting Information S1, from M_2 to K_2), and 1.6%–7.8% along the US coastline (Figure S2a in Supporting Information S1). The Root Mean Square Error between accurate ocean tidal levels and interpolated tidal levels is 0.023 m in San Francisco (Figure S2b in Supporting Information S1). Considering the differences in amplitudes and reconstructed tidal levels are small, the daily high-low data is included in our analysis and interpolated to hourly water levels.

Hourly water levels are decomposed into five components acting on different time scales to assess their effects on HTF frequency. Following the methods used by Li et al. (2022), we derive SLR from annual MSL using singular spectrum analysis and quadratic regression; we then obtain the seasonal cycle (SC) in monthly MSL with a regression model; afterward, the interannual to decadal MSL variability (ID) is computed by employing a wavelet filter (cutoff frequency is 12–360 months) to monthly MSL (after SLR is removed); tidal anomalies (TA) are the predicted ocean tides plus local MSL relative to MHHW, where ocean tides are extracted from observed hourly water levels through tidal harmonic analysis in each calendar year; and NTRs are the residuals after the removal of tides, SC, ID, and SLR from hourly water levels. We do not consider the contribution of waves in our analysis due to the hourly interval of tidal records.

After decomposition, we remove one of the sea level components and repeat the counting process to assess its effects on HTF frequency, for example, we remove SLR from daily maximum water levels and re-count annual exceedances. As for assessing the effects of changing ocean tides on HTF frequency, we follow Li et al. (2021), subtracting the changing tides from observed water levels and adding historic tides to the residuals. The changing tides are obtained by applying harmonic analysis using the UTide package (Codiga, 2011) for each calendar year and historic tides are derived from the first 19 years of available records.

We also count HTF events that could be generated by ocean tides alone, since we find that flooding thresholds could be exceeded by high tides during the peak of the nodal cycle (Li et al., 2022; Sweet et al., 2018). Nodal modulation is a slow variation of the amplitude of diurnal or semidiurnal ocean tides over a period of 18.61 years (Peng et al., 2019). We observe an 18.6-year cycle in the magnitude of the lunar diurnal tide, since the diurnal tides are directly related to the declination of the moon above the Earth's equator. Semidiurnal tides are also affected, but to a lesser extent (X. Feng, Tsimplis, & Woodworth, 2015). The nodal cycles that modulate diurnal and semidiurnal tides are out of phase, so that when diurnal tides reach high peak values, the semidiurnal tides are at the lowest of their nodal cycle (McKinnell & Crawford, 2007). To estimate the uncertainty in our results, we add errors (one sigma) to the reconstructed ocean tidal levels and repeat the counting process. The errors in reconstructed tidal levels are obtained from the UTide package through error propagation rule (Ku, 1966).

3.2. Cumulative Losses to HTF

The cumulative exposure to HTF can be computed based on the exposure to flooding as a function of water levels (Moftakhari, AghaKouchak, et al., 2017). Due to the difficulty of linking actual exposure to water levels, we use loss ratio curves derived from the Dynamic Interactive Vulnerability Assessment model (Hinkel & Klein, 2009) as a proxy. The loss ratio C is a function of inundation depth Z, namely $C_{(Z)} = \frac{Z}{Z+2}$ (Fang et al., 2020), which is based on information from local insurance companies. The cumulative loss ratios are then estimated for each flood type (i.e., minor, major, and extreme) by integrating over the respective range of probabilities:

$$\begin{cases} C_{minor} = \int_{Z=0}^{Z_{0.5}} C_{(Z)} P_{(Z)} dz \\ C_{major} = \int_{Z_{0.5}}^{Z_{0.95}} C_{(Z)} P_{(Z)} dz \\ C_{extreme} = \int_{Z_{0.95}}^{Z \to +\infty} C_{(Z)} P_{(Z)} dz \end{cases} \quad (2)$$

where Z represents the daily highest water levels above the HTF threshold (the inundation depth); $Z = 0$ represents the HTF threshold; $Z \to +\infty$ denotes the maximum observed water levels over the analysis period; $Z_{0.5}$ and $Z_{0.95}$ denote the 50th and 95th percentiles of Z, respectively. C_{minor}, C_{major}, and $C_{extreme}$ represent cumulative loss ratios for different flooding categories. $C_{(Z)}$ denotes the loss ratio at variable Z while $P_{(Z)}$ denotes probability as

a function of Z. It should also be noted here that we use minor flooding to represent HTF, to be consistent with Moftakhari, AghaKouchak, et al. (2017). Hence, minor flooding and HTF represent the same thing.

The cumulative hazard index, which is a relative measure of losses of coastal communities from HTF compared to losses from infrequent flooding, is defined by

$$\text{Cumulative hazard index} = \frac{C_{minor} - C_{extreme}}{C_{minor} + C_{extreme}} \tag{3}$$

Note that we made some modifications to the method proposed by Moftakhari, AghaKouchak, et al. (2017): (a) we use loss ratio as a proxy instead of actual property exposure curves since the data required to derive the actual curves was not available or accessible; (b) we compute cumulative loss ratios based on daily highest water levels instead of hourly water levels because an extreme flooding event usually starts with minor flooding; (c) we set the elevation of the threshold as the starting point of the loss ratio curve, rather than the mean higher high water (MHHW) because water levels above MHHW may not lead to inundation.

There is a concern that the short records available for many tide gauges (often 1976–1997) could skew the results. We thus take Hongkong, with a long continuous record, as an illustrative example to examine how short record lengths affect cumulative losses (which are estimated based on extreme sea levels). Extreme sea levels are defined as the daily highest water levels above HTF threshold. We then compare the distributions of extreme sea levels between 1976–1997 and 1951–2018 in Hongkong. As shown in Figure S3 in Supporting Information S1, the distributions show some small differences between these two periods (Figures S3a–S3m in Supporting Information S1), especially when SLR leads to more threshold exceedances (Figures S3c–S3m in Supporting Information S1). For other sites without sufficient observed data to estimate distribution differences, we use simulated total water levels from C3SCDS (Muis et al., 2022), which provides total water levels from 1950 to 2018 along the China coastline. The distribution differences (1979–1997 vs. 1950–2018) are small in Lianyungang (Figure S3 in Supporting Information S1) and other sites (not shown). To estimate the uncertainty in loss ratios, the distribution differences in simulated water levels between the two periods are used to correct the distributions of observations, and we repeat the cumulative loss ratio analysis.

3.3. Contributions of Sea Level Components During HTF

The relative contributions of sea level components (or processes) during HTF are defined by:

$$\text{Contribution} = \frac{\text{Component}}{\text{HTF}_{\text{threshold}} - \text{MHHW}} \times 100\% \tag{4}$$

Several methods are employed to obtain the sea level components (Section 3.1). For every HTF event, we can calculate the contribution of each sea level process. The sum of contributions exceeding 100% indicates that the superposition of these components would lead to HTF, for example, the sum of TA + NTR could exceed 100%, or TA alone could already exceed 100%.

3.4. Projection of HTF Frequency

Future frequencies of HTF days are projected using the statistical model from Thompson et al. (2019), who hypothesized that the probability distribution that determines the number of exceedance days during a given year could be described as a function of two variables: annual MSL and annual amplitude of astronomical tides. A summary of the statistical method is provided below; for more details please refer to Thompson et al. (2019).

1. Model the relationship between HTF frequency and the sum of two variables above a given threshold (hereafter, Δ_{99}) through empirical cumulative distribution functions. For every Δ_{99}, we build an empirical cumulative distribution function with 0.01 m width near Δ_{99} (Figure S5 in Supporting Information S1), and obtain the 50th percentile of HTF frequency.
2. Predict the annual MSL and the amplitude of astronomical tides. Annual MSL consists of SLR and ID, the predictions of which are obtained from the NASA projection tool and a Gaussian process model, respectively. Future astronomical tides are predicted by tidal harmonic analysis (Codiga, 2011), which uses the tidal harmonic constants derived from the latest available 19-year window as input.

10.1029/2022EF003225

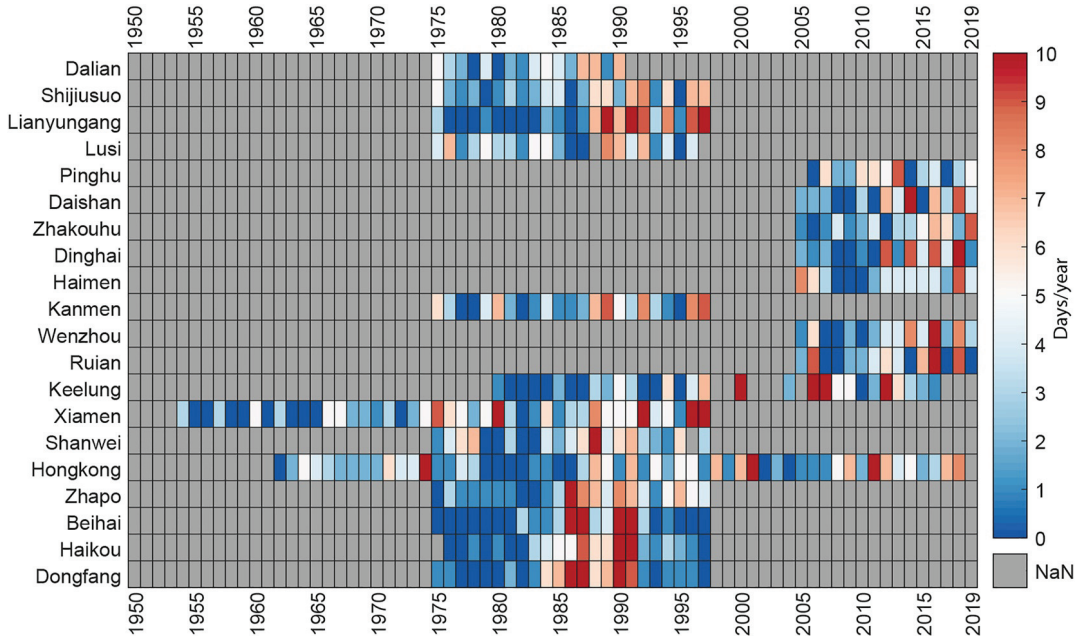

Figure 2. Annual counts of daily maximum water levels exceeding high-tide flooding (HTF) thresholds. Stations are organized from north to south (nos. 1–20). Colorbar represents the number of HTF days per year. Gray boxes indicate insufficient data (i.e., either no data or less than 75% of hourly values) to implement tidal harmonic analysis.

3. Input annual MSL and predicted astronomical tides to the empirical cumulative distribution function in step 1 to predict HTF frequency.
4. Repeating the Gaussian process 1,000 times, we obtain 1,000 HTF frequencies for the 50th percentile; the mean values of the 1,000 simulations are the final output of the HTF frequency prediction. We repeat the prediction process but using the 17th and 83rd percentiles of SLR provided by NASA. The results are regarded here as the uncertainty of predicted HTF frequency.

We made some modifications to the method proposed by Thompson et al. (2019): (a) we use empirical cumulative distribution functions to build the statical model instead of the beta-binomial distribution, since the former is simpler to implement and the differences in predicted HTF between these two methods are relatively small in San Francisco (Figures S4e and S4f in Supporting Information S1, the median is 16 days, and the 5th–95th percentile range is 0–64 days); (b) we use 0.01 m as bin width rather than 0.02 m, because tide prediction errors are in the order of millimeters to a centimeter, and we want to cover that range. Comparisons are made between different bin widths (0.01/0.015/0.02/0.025 m), the differences of which are ±5 days (Figures S4a–S4d in Supporting Information S1).

The key factor of the prediction model lies in the distribution of HTF frequency. We then compare the distributions of HTF days between 1976–1997 and 1951–2018 in Hongkong and San Francisco (Figure S5 in Supporting Information S1) to test whether the distributions are different between these two periods. The distributions show differences between the two periods over time (Figures S5b and S5e in Supporting Information S1), indicating that using short records could lead overestimation or underestimation of the HTF frequency. However, the differences are small, −15 to 5 days in Hongkong, and −7 to 8 days in San Francisco, CA (Figures S5c and S5f in Supporting Information S1). These results indicate that tidal gauges with short records can in general be used in the prediction section, while keeping in mind that these uncertainties exist.

4. Results

4.1. Changes in HTF Frequency

We start with the annual counts of daily maximum water levels that have exceeded the threshold levels in each calendar year. Hongkong and Xiamen with long-term records provide illustrative examples, clearly showing an increasing frequency of HTF over time (Figure 2). The 5th–95th percentile ranges of doubling times in HTF

frequencies at Xiamen and Hongkong are 11.5–37.4 years (the median is 17.5 years) and 23.6–796 years (the median is 45.9 years), respectively. Most of the other sites with record lengths around 20 years also experienced increases in HTF (with median/mean doubling times of 13.9/17.7 years), but these trends should be interpreted with care due to short record lengths and the fact many records ended in 1997 when a strong El Niño affected sea level in the region. The South China Sea coast (e.g., Beihai) is an exception where trends are negligible or even negative; this is because of a cluster of years with many exceedances around 1987, when the nodal cycle that modulates ocean tides reached its peak. The trends in HTF days stay positive if we count annual HTF days for the meteorological year (May-April; Figure S6 in Supporting Information S1), which includes the entire storm season. SLR contributed to the increased frequency of HTF (19%–34% of all HTF days would not occur if the SLR is removed from observations). Sites on the southeast coast of China, such as Hongkong and Haikou, are greatly impacted by local MSL (Figure S7 in Supporting Information S1). Attention should be paid to these sites as the China Sea Level Bulletin (Ministry of Natural Resources of the People's Republic of China, 2021) reported unprecedented magnitudes of SLR along the China coastline.

Changes in tides are detected along the China coastline (Devlin et al., 2017; X. Feng, Tsimplis, & Woodworth, 2015), and decreases in the tidal range during peaks of nodal cycle (Figure S8a in Supporting Information S1) have reduced the occurrences of HTF at almost half of the sites (8 in 20) (Figure S8c in Supporting Information S1, blue circles). Changes in HTF frequency caused by evolving tides are small in the remainder of sites, and they are not significantly different from zero at the one-sigma confidence level.

We further analyze how many HTF days could have occurred from astronomical tides alone. An illustrative example in Hongkong is shown in Figure S9 in Supporting Information S1, where we show the HTF days that could be generated by tides alone under different SLR scenarios. Figure 3 shows the percentage of purely tide-induced HTF days versus all HTF days. Most sites have no HTF days caused by astronomical tides alone over the analysis period, except for Zhapo to Dongfang showing relatively high percentages (12.3%–114.3%). An extreme case occurs in Beihai, where the percentage for present-day (left column in Figure 3) is higher than 100%, indicating that all observed HTF days could have been caused by high tides alone. Additional HTF events that could have occurred due to tides were prevented by negative contributions of other components, for example, negative NTR. The percentages increase with SLR (along the *x*-axis in Figure 3). The South China Sea coast (i.e., Zhapo, Beihai, Haikou, and Dongfang) will experience the fastest increase in the percentage of tide-driven HTF events due to SLR, as indicated by the transition from blue to red in Figure 3.

4.2. Cumulative Loss Ratios

The cumulative flooding losses are estimated based on the loss ratio of flooding as a function of water levels, which is then integrated over the range of probabilities for different flooding types (i.e., minor, major, and extreme). Minor flooding and HTF represent the same thing in our analysis, but major flooding in our analysis (also in Moftakhari, AghaKouchak, et al., 2017) is different from the definition used by NOAA (Sweet et al., 2018). Here, we use terminology consistent with Moftakhari, AghaKouchak, et al. (2017), namely minor/major/extreme flooding (instead of minor/moderate/major used by NOAA). The differences in inundated area and depth between extreme flooding and HTF at Xiamen are shown in Figure S10 in Supporting Information S1. The cumulative loss ratio of HTF in Xiamen (19.3% of total loss) is comparable to that of extreme flooding (17.2% of total loss) (Figure 4, pie chart), although the frequency of HTF is ∼10 times greater than that of extreme flooding (Figure 4, blue bar vs. red bar). Like Moftakhari, AghaKouchak, et al. (2017), we also find that major flooding leads to the highest cumulative loss ratios (63.5% of total loss), mainly due to its higher loss ratio relative to HTF and significantly higher frequency compared to extreme flooding. The cumulative hazard index, defined as a relative measure of coastal community exposure to HTF versus infrequent floods, reaches 0.05 in Xiamen. This index fluctuates around 0 when we conduct sensitivity analysis like changing the flooding thresholds (Figure S7 in Supporting Information S1), indicating that the results are robust. According to Equation 3, index values close to 0 indicate that cumulative losses of HTF in Xiamen are of the same order of magnitude as those from extreme flooding.

We extend the same analysis to other sites and obtain a map for cumulative hazard indices for the entire China coastline. As shown in Figure 5, most sites show negative values for the cumulative hazard index, except Dongfang (0.27) and Xiamen (0.06) located on the south coast. We would see more sites with higher values under SLR. For example, the index gets higher for half the sites when considering 0.1 m of SLR, which is similar to the actual SLR since 1997 (end of available tide gauge records in many locations) if we assume the local mean SLR followed the global rate of 3.1 mm/yr (Dangendorf et al., 2019). We thus conclude that the increases in cumulative losses

10.1029/2022EF003225

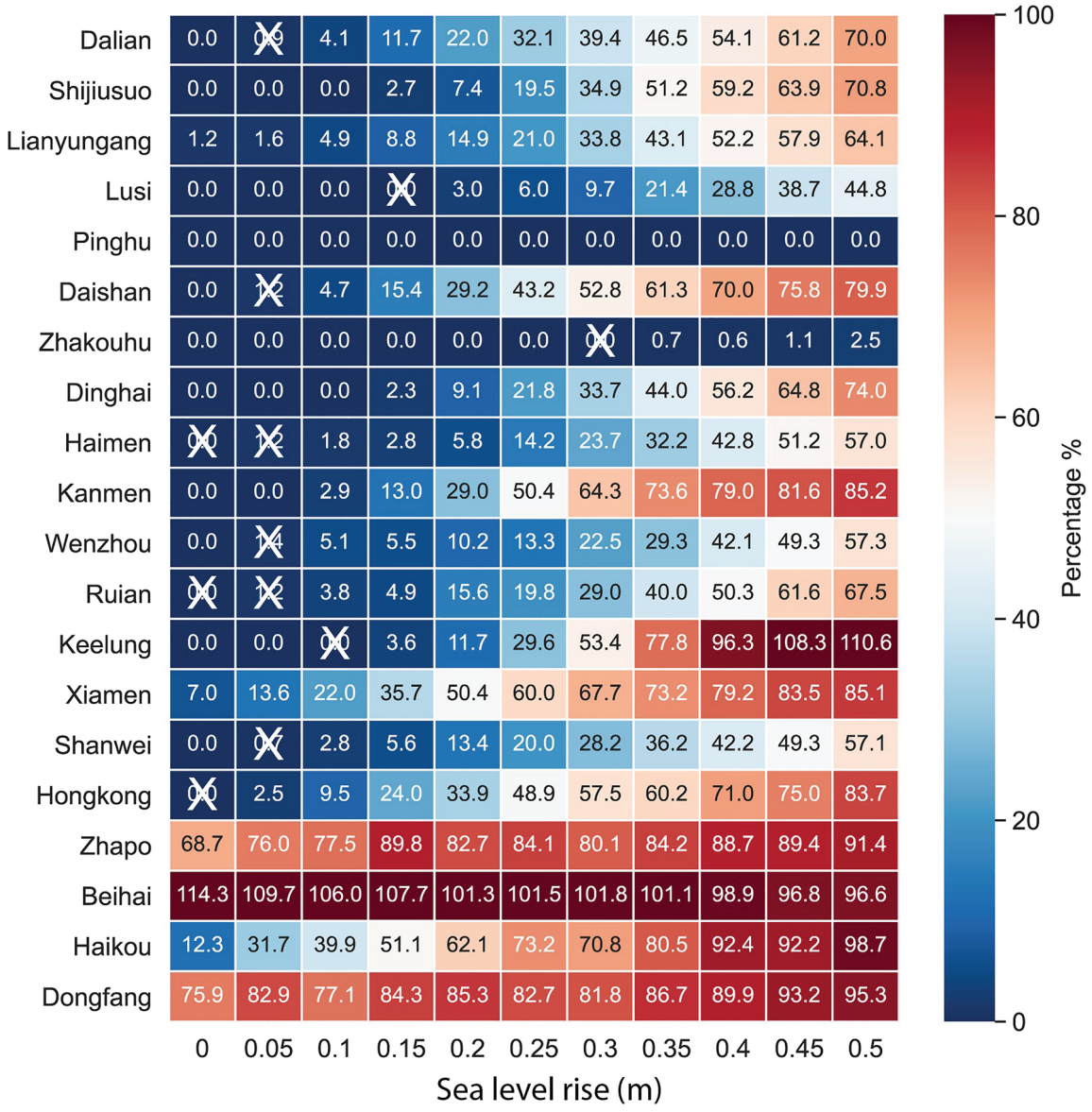

Figure 3. Percentages of high-tide flooding (HTF) days from astronomical tides alone to the total number of HTF days under different sea-level rise (SLR) scenarios (relative to the end of the observational record). Colorbar and numbers in the boxes represent the percentage. Percentages close to 0 means no HTF could be created by astronomical tides alone, whereas 100% means all HTF days could occur purely due to high tides. Percentages higher than 100% indicate that the negative contributions of other components prevented HTF days which could have been generated by tides alone. Locations are organized from north to south. Results under 0-m SLR denote the results derived from observations. Squares with crosses denote that results were not significantly different from 0 at the 90th percentile confidence interval.

of HTF may be larger than those of major flooding events in almost half of the sites during the past two decades. This trend will continue with ongoing SLR (Figure 5); 85% (17 out of 20) of sites show increases in the index, along with 9 sites exhibiting positive values. The index values also change when we use other thresholds (Figure S11 in Supporting Information S1), but the general conclusions hold. These results indicate that the cumulative losses of HTF for many sites were of the same order of magnitude (or even larger) as those caused by extreme events over the available records lengths, and this will become even more apparent under SLR.

4.3. Contributions of Sea Level Components During HTF

The still water levels are decomposed into five sea level components (i.e., SLR/ID/SC/TA/NTR) with methods mentioned in Sections 3.1 and 3.3. We then compute the relative contributions of different components to HTF. Figure 6 shows the contributions of different components expressed as percentiles (5th–95th percentile,

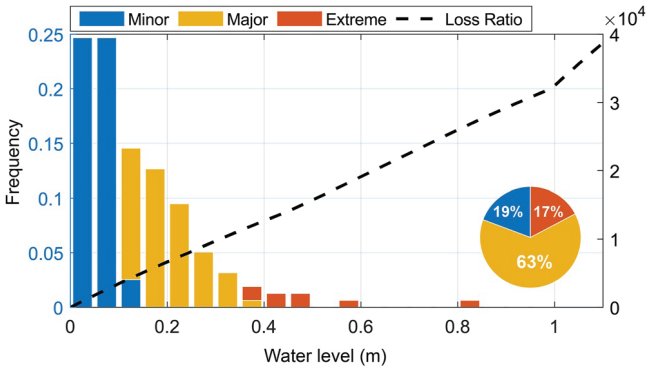

Figure 4. Loss ratios for minor (blue), major (yellow), and extreme flooding (red) in Xiamen (Global Sea Level Observing System ID: 274). Bars represent the empirical probability density of the daily highest water level above the flooding threshold (99th of daily highest water levels, equal to 6.780 m). Flooding events are classified into minor (blue), major (yellow), and extreme flooding (red), with exceedance probability greater than 0.50, between 0.05 and 0.50, and less than 0.05 of daily highest water levels above the threshold, respectively. In total, 158 flooding days occurred over the analysis period (1954–1997). The black dashed line against right *y*-axis represents the loss ratio acting as a function of water levels above the flooding threshold. The black dashed line is obtained by summing the loss ratios at all inundated grid points near the tidal gauge in the digital elevation model. Inserted pie chart denotes the relative contribution of different flood types to the total loss.

and median) at 20 locations along the China coastline. For example, Xiamen experienced a total of 158 HTF days over the analysis period, with TA being the dominant component (Figure 6, purple bar) for most of the HTF days. The contributions of TA range from 41% to 94% (the median is 75%) in Xiamen. The upper range of TA is close to 100%, indicating that TA alone could push water levels close to the HTF threshold. NTR contributes between 2% and 66% (median is 22%) to HTF. In contrast, NTR plays the most important role (contributes between 30% and 123%, median is 61%) in high water levels leading to HTF at Shanwei. TA in Shanwei plays a secondary role (−23% to 74%) to HTF, which also makes negative contributions because the surges occur randomly on top of tides.

TA and NTR are the two main contributors to HTF. TA contributes the most from Dalian to Lianyungang (Figure 6, purple circles are highest). It then becomes small in Hangzhou Bay (from Pinghu to Dinghai), where the contribution of NTR dominates (40.5%–109%). Further south, TA dominates again from Haimen to Dongfang, except in Keelung, Shanwei, and Hongkong, where the contributions of TA are smaller than NTR. Extreme contributions of TA occur along the South China Sea coast (e.g., Zhapo, Beihai, and Dongfang), with values up to 100%. This implies that HTF in this area can arise from astronomical tides alone. SC contributes less to HTF than NTR and TA at most sites (yellow circles below purple and green), but SC can contribute 11%–46% (median, 37%) to individual HTF events in Keelung (Figure 6). ID and SLR show smaller contributions (most sites <10%) than other components.

The analysis outlined above resulted in a new data set of the relative contribution of different sea-level processes to HTF. We then identify the importance of a particular component by analyzing the minimum number of sea level components (in addition to SLR) needed to exceed the HTF threshold. Components contributing the most are counted first in the counting process. HTF created by two components in Xiamen shows the largest increase in frequency (34 days) between the beginning 19-year window (1954–1972) and the latest 19-year window (1979–1997) (Figure S12 in Supporting Information S1, blue bar). Additionally, Xiamen experienced HTF threshold exceedances by two components in 1988, 1996, and 1997 (red bar), whereas from 1954 to 1980, there was no HTF created by two components. HTF frequency changes in Hongkong show similar results, but with a drop in the number of HTF events where all five components were required to cross the threshold. This means the HTF which was triggered by five components in the past, is now caused by the combination of four or only three components. We do not extend the above analysis to the other sites due to their short record lengths, but similar results would likely be found at other locations as SLR will narrow the gap between high water levels and flooding thresholds.

4.4. Projection of HTF

Decision makers need reliable information on how SLR and other factors could affect the frequency of HTF in the coming decades along the China coastline. Following the work of Thompson et al. (2019), we use a statistical model to predict future HTF frequencies. For example, Xiamen will experience more HTF days under different warming scenarios (Figure 7a). More rapid increases in HTF frequency are expected in the 2050s and 2080s due to the nodal cycle that modulates ocean tides and the general rise in sea level. Besides, there is also a sub-decadal variation in HTF frequency, that is, two peaks per decade. This is related to the half period of lunar perigee precession, which is 4.4 years (Ray & Foster, 2016). In the coming 30 years, Xiamen will likely experience less than 30 ± 15 HTF days under all SLR scenarios. By 2100, however, the frequency under SSP5-8.5 is almost three times larger than that under SSP1-1.9 (Figure 7a, blue vs. red line), implying a warming earth system without additional climate policy will greatly change the HTF frequency in the future. Other sites show similar changes in predicted HTF frequencies, in which the nodal cycle, perigee cycle, and general increase in sea level are the main drivers of the projected changes.

The probabilistic projections of exceedance days should be used with caution as extreme weather events, for example, could lead to much higher numbers of exceedances in a given year. Thus, besides focusing on the

10.1029/2022EF003225

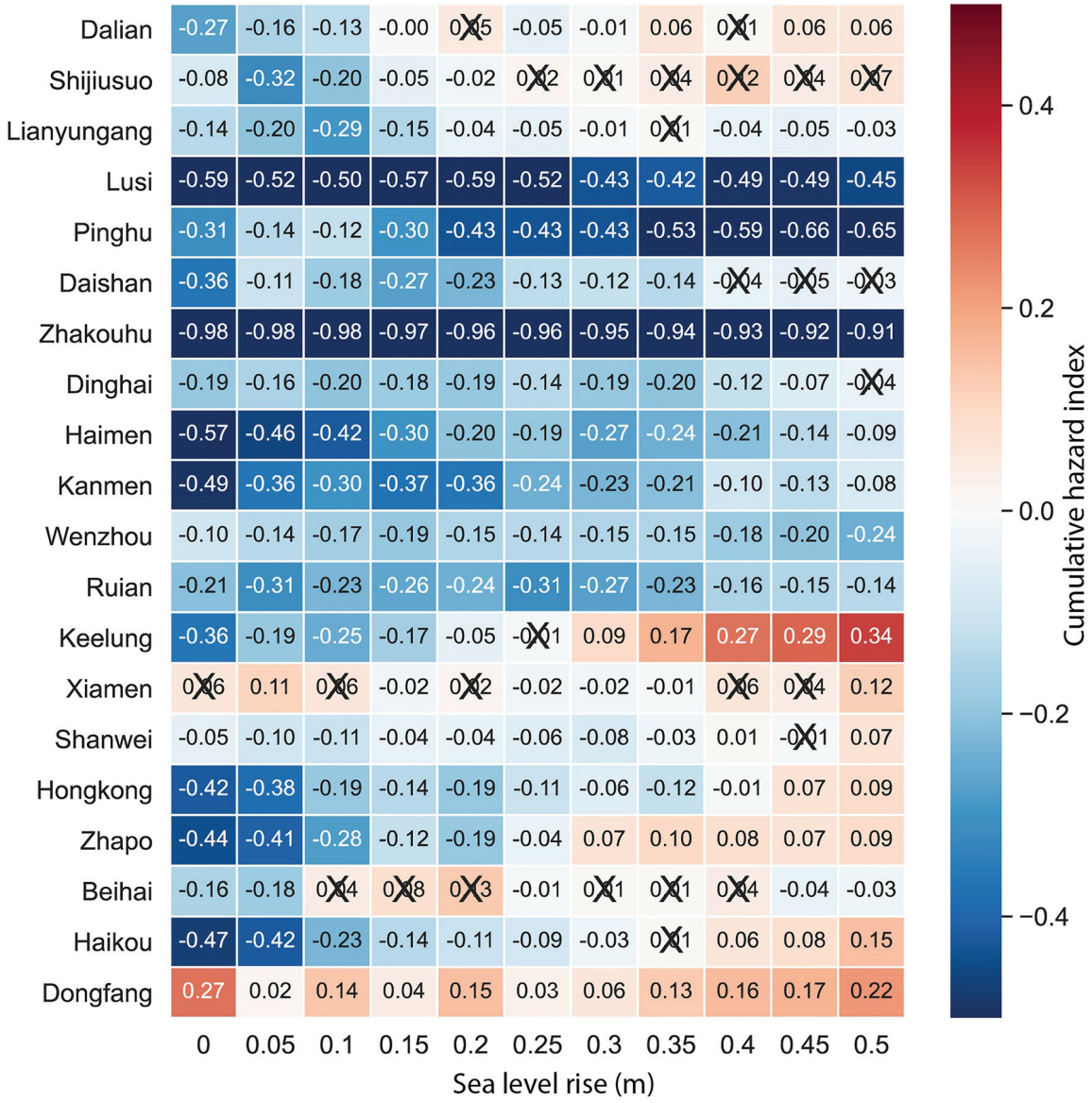

Figure 5. Cumulative hazard index under sea level rise. Color bar and numbers in the boxes represent the cumulative hazard index. Positive values are shown in red (i.e., the cumulative losses from high-tide flooding (HTF) are bigger than those from extreme flooding), and negative values are shown in blue (i.e., the cumulative losses from HTF are smaller than those from extreme flooding). An index close to −1 means the cumulative losses associated with HTF are negligible relative to the ones caused by extreme events, whereas close to +1 means the cumulative losses from extreme events are negligible compared to HTF losses. Locations are organized from north to south. Results under 0-m sea-level rise (SLR) denote the results derived from observations. Squares with crosses denote that results were not different from 0 when considering the uncertainties due to short record lengths.

number of exceedance days to expect in a specific year, we also assess the start year when a site transitions to chronic HTF, which is defined by 9 out of 10 continuous years experiencing more than 50 HTF days (Thompson et al., 2019). At Xiamen, for example, chronic HTF could transition to chronic as early as the mid-2060s, but it may also not start to happen this century under SSP2–4.5 (Figure 7a, blue horizontal error bar). The start year of chronic HTF occurs earlier under a stronger warming scenario, between the early 2060s and mid-2080s (Figure 7a, red horizontal error bar). The time lag between the first year showing 50 HTF days and 9 in 10 years showing 50 HTF days is 16 and 10 years under the SSP1–1.9 and SSP5–8.5 scenarios, respectively. We extend the same analysis to other sites and derive a map (Figure 7b) for the start years of chronic HTF under SSP2–4.5 (the moderate warming scenario). Haikou, for example, will likely start experiencing chronic HTF between the late 2030s and mid-2050s. Most sites (17 in 20) transition to chronic HTF after 2060 under SSP2–4.5. On average,

10.1029/2022EF003225

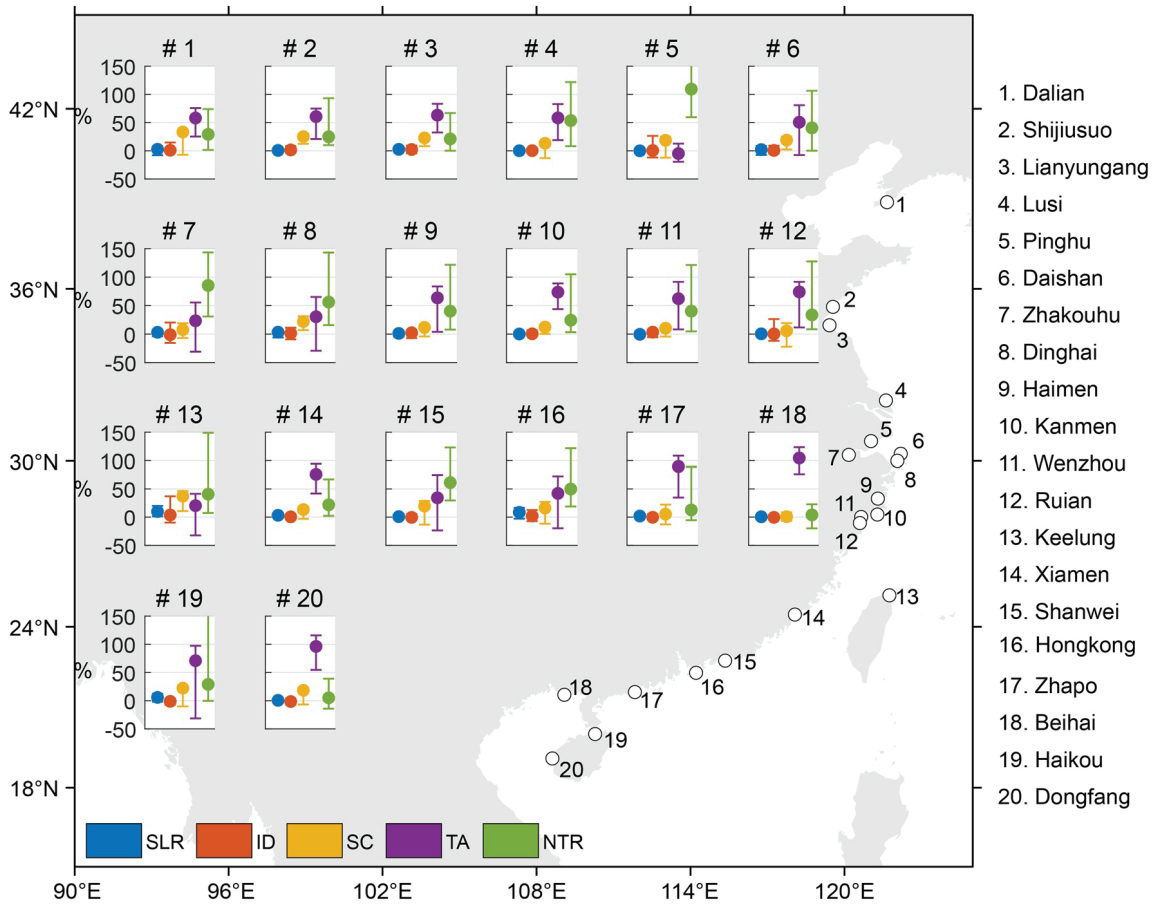

Figure 6. Contributions of different sea-level components to still water levels during high-tide flooding (HTF) expressed in percent. Color denotes different sea level components, while bars represent relative contributions. The range of bar is from 5th to 95th percentiles, with the circle denoting the median. Sea-level rise (SLR) is shown in cyan, while the interannual to decadal mean sea level (MSL) variability (ID) is in orange, seasonal cycle in monthly MSL (SC) in green, tidal anomaly (TA) in blue, and nontidal residual (NTR) in red. Locations are organized from north to south (with increasing numbers).

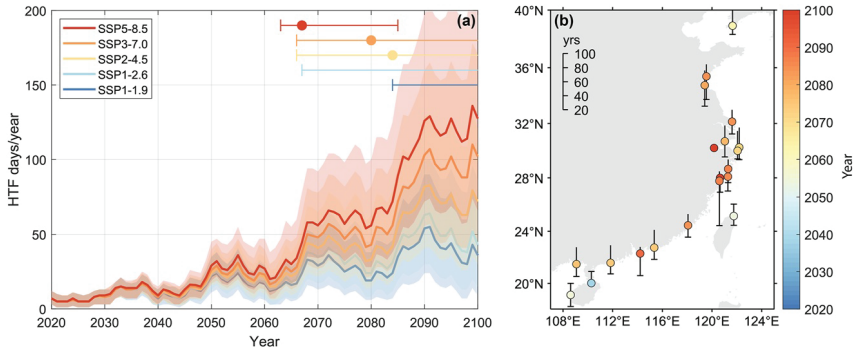

Figure 7. (a) Prediction of high-tide flooding (HTF) days under different sea-level rise (SLR) scenarios in Xiamen. Solid lines represent the most likely (median) annual counts of HTF days; shading represents likely (17%–83%) probability intervals. Horizontal error bars denote the start years of chronic HTF with circles representing median values and bars representing 5th–95th percentiles. Chronic HTF is defined as 9 out of 10 continuous years experiencing more than 50 HTF days. SLR scenarios from SSP1–1.9 to SSP5–8.5 denote very low (1.9)/low (2.6)/intermediate (4.5)/high (7.0)/very high (8.5) of greenhouse gas emissions according to the Sixth Assessment Report of the IPCC (Arias et al., 2021). (b) Start year of chronic HTF under SSP2–4.5. Error bars represent the 5th–95th percentile ranges of the start years, while the colorbar represents the median start year. Error bars without horizontal lines indicate that the start year occurs after 2100. Red colors indicate the transition to chronic HTF occurs later, while blue colors indicate an earlier transition.

the South China Sea coast transitions earlier than other coasts from Dalian to Xiamen (Figure 7b, yellow vs. red circles).

5. Discussion

Policymakers are acutely aware of the grave consequences of extreme flooding events like those caused by typhoons (Moftakhari, Salvadori, et al., 2017). Here we show that the cumulative losses from HTF could be comparable to those from extreme events along the China coast, for example, the HTF and extreme events account for 19% and 17% of loss ratios, respectively. We acknowledge that the HTF thresholds used in our study are not the actual flooding thresholds for coastal cities. We thus tested different ways to derive reasonable HTF thresholds. They are: (a) 99th percentile of daily highest water levels, which is around 99th of hourly water levels (Haigh et al., 2010); (b) the 2-year return water levels (China National Standard); and (c) interpolated threshold based on diurnal tidal ranges (Sweet et al., 2018), usually ∼0.5 m above local MHHW. In addition, we considered a threshold that is 0.3 m above local MHHW (Ezer & Atkinson, 2014), which generally leads to lower values than the ones derived with the NOAA interpolation approach (not shown). Since the increase in MSL equals a reduction in the threshold of HTF, results derived by Ezer and Atkinson (2014) for lower thresholds will eventually occur under SLR. The phenomenon that cumulative impacts of minor events are comparable to that of extreme events is not limited to flood losses. B. Chen et al. (2020) pointed out that the cumulative deaths of "extensive" floods are comparable to those of "intensive" events in the long run, although their definition of minor flooding is different from ours.

We are also aware that the cumulative loss ratios in our analysis are rough estimates. There is room for improvement: (a) use DEMs with higher spatial resolution and vertical accuracy; (b) exclude gird points without any property on them (e.g., roads); (c) employ loss ratio curves that are more representative of cities at our study sites as the loss ratio curve derived from DIVA is designed for the United Kingdom and may not be suitable for China; and (d) considering hydrodynamic effects when computing inundation.

Increasing HTF frequency has been reported in the United States (Moftakhari et al., 2015; Sweet et al., 2018; Vitousek et al., 2017), Australia (Hague et al., 2022; Lowe et al., 2021), and Europe (Vousdoukas et al., 2017), posing threats to low lying coastal cities. Our results show that the China coast is facing similar HTF issues, in large parts due to SLR. Although using short records may not change our overall conclusions the sensitivity analyses in Section 3 showed, metrics like the doubling time may change when longer records are considered. In particular, the records ending in 1997 when a strong El Niño led to significant sea level variability could be impacted.

Cities which already experienced HTF triggered by astronomical tides alone (or will experience it soon) are facing severe coastal flooding problems due to frequent HTF events. Cities along the US coastline like Boston and San Francisco already experienced HTF days caused by tides alone (Li et al., 2022; Ray & Foster, 2016; Sweet et al., 2018) and similar examples are found in this study along the South China Sea coastline. Just as local media in Beihai reported, several HTF events happened during the timing of high astronomical tides. Beihai provides a very extreme case where >100% of HTF days could be caused by astronomical tides alone, far higher than the rest of the sites analyzed here, as well as sites studied in the United States (<30% of all HTF days).

We also compute the contributions of components during HTF. We identify strong regional coherence in certain components like TA and NTR during HTF. Examples include the coast of South China Sea, where TA plays a major role (especially in Beihai and Dongfang) and NTR is more influential in the Hangzhou Bay. These results are in accordance with previous studies, which analyzed the effects of different processes on extreme sea levels (e.g., Idier et al., 2019; Melet et al., 2018; Merrifield et al., 2013; Rueda et al., 2017). SC contributes the most to HTF in Dalian, which is consistent with the results that the amplitude of SC is large in this region (Amiruddin et al., 2015; X. Feng, Tsimplis, Marcos, et al., 2015).

HTF was predicted with a statistical model using a range of input variables. Ocean tides, one of the input variables, are predicted with the latest available tidal harmonic constants. The prediction of tides could be improved if we consider: (a) the actual nodal cycle correction, which is not in accordance with the theoretical correction (Li et al., 2021; Ray & Talke, 2019); and/or (b) the long-term changes in tidal constituents along the China coastline (X. Feng, Tsimplis, & Woodworth, 2015).

Data constraints (e.g., Qinhuangdao/Tanggu where the data are not publicly available) prevent the analysis of HTF in many locations. The tidal records ending in 1997 also limit the assessment of HTF for present conditions. A notable example is Xiamen, a new first-tier city being an important population and economic center situated on the southeastern coast of China. Our results outline the potential impacts of HTF at the community level and can aid policymakers in planning adaptation accordingly. Overall, we advocate that more attention is paid to HTF (beyond analyzing extreme flooding events) along the China coastline.

6. Conclusions

We build on previous works to analyze HTF changes in the past and future for the China coastline, where previous assessments almost exclusively focused on extreme flooding events. Our results show that the frequency of HTF has increased along the China coastline over the periods where tide gauge data is available, in large parts due to SLR. Notably, the cumulative losses from HTF are found to be comparable to those from extreme events in many locations already under present-day conditions, and HTF losses will outpace those from extreme flooding in more locations with continuing SLR. Similar to major cities along the US coastline, several locations along the China coast already experience HTF that is solely caused by tides (Li et al., 2022; Ray & Foster, 2016; Sweet et al., 2018). Beihai provides an extreme example where all HTF days in the past could have been caused by astronomical tides alone, whereas the relative number of HTF events that could have been caused only by tides is smaller for the rest of the sites in our study region (and in the United States). Our results concerning potential changes in HTF frequency demonstrate how quickly exceedance days above a threshold in the China coast will transition from occasional to chronic. This highlights the necessity to plan for adaptation investments proactively, because the time lags between deciding to adapt and having it implemented could be longer than the short time periods it will take for HTF to transition from occasional to chronic.

Conflict of Interest

The authors declare no conflicts of interest relevant to this study.

Data Availability Statement

The data are available at https://gesla787883612.wordpress.com/ (hourly water level), https://figshare.com/articles/dataset/High_low_tide_record_along_the_China_coastline/20510562 (daily high and low water level), https://www.psmsl.org/data/obtaining/complete.php (annual mean sea level), https://sealevel.nasa.gov/ipcc-ar6-sea-level-projection-tool (sea level rise projection), https://search.earthdata.nasa.gov/search?q=ASTER%20GDEM%20v3 (DEM data), https://www.aviso.altimetry.fr/en/index.php?id=3622 (mean dynamic ocean topography), https://cds.climate.copernicus.eu/cdsapp#!/dataset/sis-water-level-change-timeseries-cmip6?tab=overview (simulated total water levels), and Matlab code used for the sea level decomposition can be obtained at Github: https://github.com/CoRE-Lab-UCF/Sea-level-components-and-contribution.

Acknowledgments
The authors thank the editor and two anonymous reviewers for their constructive comments. This work was supported by the Ministry of Science and Technology of the People's Republic of China (Grant 2011YQ120045). T.W. acknowledges support from the NASA's Sea Level Change Team (Award number 80NSSC20K1241) and the National Science Foundation (Award numbers 1854896 and 2141461). J.F. acknowledges the National Natural Science Foundation of China (Grant 42001096). T.J. acknowledges support from the Jiangsu and Lianyungang Science Foundation (Grants JSZRHYKJ202201, 2020058, and LYG06521202131). The authors thank the projection authors for developing and making the sea-level rise projections available, multiple funding agencies for supporting the development of the projections, and the NASA Sea-Level Change Team for developing and hosting the IPCC AR6 Sea-Level Projection Tool.

References

Amiruddin, A. M., Haigh, I. D., Tsimplis, M. N., Calafat, F. M., & Dangendorf, S. (2015). The seasonal cycle and variability of sea level in the South China Sea. *Journal of Geophysical Research: Oceans*, *120*(8), 5490–5513. https://doi.org/10.1002/2015JC010923

Arias, P., Bellouin, N., Coppola, E., Jones, R., Krinner, G., Marotzke, J., et al. (2021). Climate change 2021: The physical science basis. Contribution of working Group14 I to the sixth assessment report of the intergovernmental panel on climate change. Technical Summary Retrieved from https://www.ipcc.ch/report/ar6/wg1/

Burgos, A. G., Hamlington, B. D., Thompson, P. R., & Ray, R. D. (2018). Future nuisance flooding in Norfolk, VA, from astronomical tides and annual to decadal internal climate variability. *Geophysical Research Letters*, *45*(22), 12432–412439. https://doi.org/10.1029/2018gl079572

Chen, B., Shi, F., Lin, T., Shi, P., & Zheng, J. (2020). Intensive versus extensive events? Insights from cumulative flood-induced mortality over the globe, 1976–2016. *International Journal of Disaster Risk Science*, *11*(4), 441–451. https://doi.org/10.1007/s13753-020-00288-5

Chen, Y., Huang, W., & Xu, S. (2014). Frequency analysis of extreme water levels affected by sea-level rise in east and southeast coasts of China. *Journal of Coastal Research*, *68*(10068), 105–112. https://doi.org/10.2112/SI68-014.1

Cheng, L., AghaKouchak, A., Gilleland, E., & Katz, R. W. (2014). Non-stationary extreme value analysis in a changing climate. *Climatic Change*, *127*(2), 353–369. https://doi.org/10.1007/s10584-014-1254-5

Cherqui, F., Belmeziti, A., Granger, D., Sourdril, A., & Le Gauffre, P. (2015). Assessing urban potential flooding risk and identifying effective risk-reduction measures. *Science of the Total Environment*, *514*, 418–425. https://doi.org/10.1016/j.scitotenv.2015.02.027

Codiga, D. (2011). *Unified tidal analysis and prediction using the UTide Matlab functions*. Graduate School of Oceanography. https://doi.org/10.13140/RG.2.1.3761.2008

Couasnon, A., Eilander, D., Muis, S., Veldkamp, T. I. E., Haigh, I. D., Wahl, T., et al. (2020). Measuring compound flood potential from river discharge and storm surge extremes at the global scale. *Natural Hazards and Earth System Sciences*, *20*(2), 489–504. https://doi.org/10.5194/nhess-20-489-2020

Dahl, K. A., Fitzpatrick, M. F., & Spanger-Siegfried, E. (2017). Sea level rise drives increased tidal flooding frequency at tide gauges along the U.S. East and Gulf Coasts: Projections for 2030 and 2045. *PLoS One*, *12*(2), e0170949. https://doi.org/10.1371/journal.pone.0170949

Dangendorf, S., Hay, C., Calafat, F. M., Marcos, M., Piecuch, C. G., Berk, K., & Jensen, J. (2019). Persistent acceleration in global sea-level rise since the 1960s. *Nature Climate Change*, *9*(9), 705–710. https://doi.org/10.1038/s41558-019-0531-8

Devlin, A. T., Jay, D. A., Zaron, E. D., Talke, S. A., Pan, J., & Lin, H. (2017). Tidal variability related to sea level variability in the Pacific Ocean. *Journal of Geophysical Research: Oceans*, *122*(11), 8445–8463. https://doi.org/10.1002/2017jc013165

Ezer, T., & Atkinson, L. P. (2014). Accelerated flooding along the U.S. East Coast: On the impact of sea-level rise, tides, storms, the Gulf Stream, and the North Atlantic Oscillations. *Earth's Future*, *2*(8), 362–382. https://doi.org/10.1002/2014ef000252

Fang, J., Lincke, D., Brown, S., Nicholls, R. J., Wolff, C., Merkens, J. L., et al. (2020). Coastal flood risks in China through the 21st century – An application of DIVA. *Science of the Total Environment*, *704*, 135311. https://doi.org/10.1016/j.scitotenv.2019.135311

Fang, J., Wahl, T., Fang, J., Sun, X., Kong, F., & Liu, M. (2021). Compound flood potential from storm surge and heavy precipitation in coastal China. *Hydrology and Earth System Sciences*, *25*(8), 1–24. https://doi.org/10.5194/hess-25-4403-2021

Feng, J., von Storch, H., Jiang, W., & Weisse, R. (2015). Assessing changes in extreme sea levels along the coast of China. *Journal of Geophysical Research: Oceans*, *120*(12), 8039–8051. https://doi.org/10.1002/2015JC011336

Feng, X., Tsimplis, M. N., Marcos, M., Calafat, F. M., Zheng, J., Jordà, G., & Cipollini, P. (2015). Spatial and temporal variations of the seasonal sea level cycle in the northwest Pacific. *Journal of Geophysical Research: Oceans*, *120*(10), 7091–7112. https://doi.org/10.1002/2015jc011154

Feng, X., Tsimplis, M. N., & Woodworth, P. L. (2015). Nodal variations and long-term changes in the main tides on the coasts of China. *Journal of Geophysical Research: Oceans*, *120*(2), 1215–1232. https://doi.org/10.1002/2014jc010312

Ferrarin, C., Lionello, P., Orlic, M., Raicich, F., & Salvadori, G. (2022). Venice as a paradigm of coastal flooding under multiple compound drivers. *Scientific Reports*, *12*(1), 5754. https://doi.org/10.1038/s41598-022-09652-5

Fox-Kemper, B., Hewitt, H. T., Xiao, C., Adalgeirsdottir, G., Drijfhout, S. S., Edwards, T. L., et al. (2021). Ocean, cryosphere and sea level change. In V. Masson-Delmotte, P. Zhai, A. Pirani, S. L. Connors, C. Péan, S. Berger, et al. (Eds.), *Climate change 2021: The physical science basis. Contribution of working group I to the sixth assessment report of the intergovernmental panel on climate change*. Cambridge University Press.

Garner, G., Hermans, T., Kopp, R., Slangen, A., Edwards, T., Levermann, A., et al. (2021). IPCC AR6 sea-level rise projections. Version 20210809. PO.DAAC. Retrieved from https://podaac.jpl.nasa.gov/announcements/2021-08-09-Sea-level-projections-from-the-IPCC-6th-Assessment-Report

Hague, B. S., Jones, D. A., Jakob, D., McGregor, S., & Reef, R. (2022). Australian coastal flooding trends and forcing factors. *Earth's Future*, *10*(2), e2021EF002483. https://doi.org/10.1029/2021ef002483

Haigh, I. D., Marcos, M., Talke, S. A., Woodworth, P. L., Hunter, J. R., Hague, B. S., et al. (2022). GESLA version 3: A major update to the global higher-frequency sea-level dataset. *Geoscience Data Journal*. *00*, 1–22. https://doi.org/10.1002/gdj3.174

Haigh, I. D., Nicholls, R., & Wells, N. (2010). Assessing changes in extreme sea levels: Application to the English Channel, 1900–2006. *Continental Shelf Research*, *30*(9), 1042–1055. https://doi.org/10.1016/j.csr.2010.02.002

Hinkel, J., & Klein, R. J. (2009). Integrating knowledge to assess coastal vulnerability to sea-level rise: The development of the DIVA tool. *Global Environmental Change*, *19*(3), 384–395. https://doi.org/10.1016/j.gloenvcha.2009.03.002

Hino, M., Belanger, S. T., Field, C. B., Davies, A. R., & Mach, K. J. (2019). High-tide flooding disrupts local economic activity. *Science Advances*, *5*(2), eaau2736. https://doi.org/10.1126/sciadv.aau2736

Holgate, S. J., Matthews, A., Woodworth, P. L., Rickards, L. J., Tamisiea, M. E., Bradshaw, E., et al. (2013). New data systems and products at the permanent service for mean sea level. *Journal of Coastal Research*, *29*(3), 493–504. https://doi.org/10.2112/jcoastres-d-12-00175.1

Hu, B., Zhou, J., Wang, J., Chen, Z., Wang, D., & Xu, S. (2009). Risk assessment of land subsidence at Tianjin coastal area in China. *Environmental Earth Sciences*, *59*(2), 269–276. https://doi.org/10.1007/s12665-009-0024-6

Idier, D., Bertin, X., Thompson, P., & Pickering, M. D. (2019). Interactions between mean sea level, tide, surge, waves and flooding: Mechanisms and contributions to sea level variations at the coast. *Surveys in Geophysics*, *40*(6), 1603–1630. https://doi.org/10.1007/s10712-019-09549-5

Ji, T., Li, G., Liu, Y., Liu, R., & Zhu, Y. (2021). Spatiotemporal features of storm surge activity and its response to climate change in the southeastern coastal area of China in the past 60 years. *Journal of Geophysical Research: Atmospheres*, *126*(4), e2020JD033234. https://doi.org/10.1029/2020JD033234

Ku, H. H. (1966). Notes on the use of propagation of error formulas. *Journal of Research of the National Bureau of Standards*, *70*(4). Retrieved from https://nvlpubs.nist.gov/nistpubs/jres/70C/jresv70Cn4p263_A1b.pdf

Li, S., Wahl, T., Barroso, A., Coats, S., Dangendorf, S., Piecuch, C., et al. (2022). Contributions of different sea-level processes to high-tide flooding along the U.S. Coastline. *Journal of Geophysical Research: Oceans*, *127*(7), e2021JC018276. https://doi.org/10.1029/2021jc018276

Li, S., Wahl, T., Talke, S. A., Jay, D. A., Orton, P. M., Liang, X., et al. (2021). Evolving tides aggravate nuisance flooding along the U.S. coastline. *Science Advances*, *7*(10), eabe2412. https://doi.org/10.1126/sciadv.abe2412

Losada, I., Reguero, B., Méndez, F., Castanedo, S., Abascal, A., & Mínguez, R. (2013). Long-term changes in sea-level components in Latin America and the Caribbean. *Global and Planetary Change*, *104*, 34–50. https://doi.org/10.1016/j.gloplacha.2013.02.006

Lowe, R. J., Cuttler, M. V. W., & Hansen, J. E. (2021). Climatic drivers of extreme sea level events along the coastline of Western Australia. *Earth's Future*, *9*(4), e2020EF001620. https://doi.org/10.1029/2020ef001620

McKinnell, S. M., & Crawford, W. R. (2007). The 18.6-year lunar nodal cycle and surface temperature variability in the northeast Pacific. *Journal of Geophysical Research*, *112*(C2), C02002. https://doi.org/10.1029/2006jc003671

Melet, A., Meyssignac, B., Almar, R., & Le Cozannet, G. (2018). Under-estimated wave contribution to coastal sea-level rise. *Nature Climate Change*, *8*(3), 234–239. https://doi.org/10.1038/s41558-018-0088-y

Menéndez, M., & Woodworth, P. L. (2010). Changes in extreme high water levels based on a quasi-global tide-gauge data set. *Journal of Geophysical Research: Oceans*, *115*(C10), C10011. https://doi.org/10.1029/2009JC005997

Merrifield, M. A., Genz, A. S., Kontoes, C. P., & Marra, J. J. (2013). Annual maximum water levels from tide gauges: Contributing factors and geographic patterns. *Journal of Geophysical Research: Oceans*, *118*(5), 2535–2546. https://doi.org/10.1002/jgrc.20173

Ministry of Natural Resources of the People's Republic of China. (2022). China mean sea level bulletin 2021. Retrived from http://gi.mnr.gov.cn/202205/P020220609556998660192.pdf

Moftakhari, H. R., AghaKouchak, A., Sanders, B. F., Allaire, M., & Matthew, R. A. (2018). What is nuisance flooding? Defining and monitoring an emerging challenge. *Water Resources Research*, *54*(7), 4218–4227. https://doi.org/10.1029/2018wr022828

Moftakhari, H. R., AghaKouchak, A., Sanders, B. F., Feldman, D. L., Sweet, W., Matthew, R. A., & Luke, A. (2015). Increased nuisance flooding along the coasts of the United States due to sea level rise: Past and future. *Geophysical Research Letters*, *42*(22), 9846–9852. https://doi.org/10.1002/2015gl066072

Moftakhari, H. R., AghaKouchak, A., Sanders, B. F., & Matthew, R. A. (2017). Cumulative hazard: The case of nuisance flooding. *Earth's Future*, *5*(2), 214–223. https://doi.org/10.1002/2016ef000494

Moftakhari, H. R., Salvadori, G., AghaKouchak, A., Sanders, B. F., & Matthew, R. A. (2017). Compounding effects of sea level rise and fluvial flooding. *Proceedings of the National Academy of Sciences of the United States of America*, *114*(37), 9785–9790. https://doi.org/10.1073/pnas.1620325114

Muis, S., Apecechea, M. I., Álvarez, J. A., Verlaan, M., Yan, K., Dullaart, J., et al. (2022). *Global sea level change time series from 1950 to 2050 derived from reanalysis and high resolution CMIP6 climate projections*. Copernicus Climate Change Service (C3S) Climate Data Store (CDS). https://doi.org/10.24381/cds.a6d42d60

Pelling, H., Uehara, K., & Green, J. M. (2013). The impact of rapid coastline changes and sea level rise on the tides in the Bohai Sea, China. *Journal of Geophysical Research: Oceans*, *118*(7), 3462–3472. https://doi.org/10.1002/jgrc.20258

Peng, D., Hill, E. M., Meltzner, A. J., & Switzer, A. D. (2019). Tide gauge records show that the 18.61-year nodal tidal cycle can change high water levels by up to 30 cm. *Journal of Geophysical Research: Oceans*, *124*(1), 736–749. https://doi.org/10.1029/2018jc014695

Ray, R. D., & Foster, G. (2016). Future nuisance flooding at Boston caused by astronomical tides alone. *Earth's Future*, *4*(12), 578–587. https://doi.org/10.1002/2016EF000423

Ray, R. D., & Talke, S. A. (2019). Nineteenth-century tides in the Gulf of Maine and implications for secular trends. *Journal of Geophysical Research: Oceans*, *124*(10), 7046–7067. https://doi.org/10.1029/2019jc015277

Rueda, A., Vitousek, S., Camus, P., Tomás, A., Espejo, A., Losada, I. J., et al. (2017). A global classification of coastal flood hazard climates associated with large-scale oceanographic forcing. *Scientific Reports*, *7*(1), 1–8. https://doi.org/10.1038/s41598-017-05090-w

Serafin, K. A., Ruggiero, P., & Stockdon, H. F. (2017). The relative contribution of waves, tides, and nontidal residuals to extreme total water levels on U.S. West Coast sandy beaches. *Geophysical Research Letters*, *44*(4), 1839–1847. https://doi.org/10.1002/2016gl071020

Shi, X., Liu, S., Yang, S., Liu, Q., Tan, J., & Guo, Z. (2015). Spatial–temporal distribution of storm surge damage in the coastal areas of China. *Natural Hazards*, *79*(1), 237–247. https://doi.org/10.1007/s11069-015-1838-z

Sweet, W. V., Dusek, G., Obeysekera, J., & Marra, J. J. (2018). Patterns and projections of high tide flooding along the U.S. coastline using a common impact threshold (Tech. Rep., NOAA NOS CO-OPS 086, 2018). Retrived from https://tidesandcurrents.noaa.gov/publications/techrpt86_PaP_of_HTFlooding.pdf

Sweet, W. V., & Park, J. (2014). From the extreme to the mean: Acceleration and tipping points of coastal inundation from sea level rise. *Earth's Future*, *2*(12), 579–600. https://doi.org/10.1002/2014ef000272

Taherkhani, M., Vitousek, S., Barnard, P. L., Frazer, N., Anderson, T. R., & Fletcher, C. H. (2020). Sea-level rise exponentially increases coastal flood frequency. *Scientific Reports*, *10*(1), 6466. https://doi.org/10.1038/s41598-020-62188-4

Tang, W., Zhan, W., Jin, B., Motagh, M., & Xu, Y. (2021). Spatial variability of relative sea-level rise in Tianjin, China: Insight from InSAR, GPS, and tide-gauge observations. *IEEE Journal of Selected Topics in Applied Earth Observations and Remote Sensing*, *14*, 2621–2633. https://doi.org/10.1109/JSTARS.2021.3054395

Thompson, P. R., Widlansky, M. J., Hamlington, B. D., Merrifield, M. A., Marra, J. J., Mitchum, G. T., & Sweet, W. (2021). Rapid increases and extreme months in projections of United States high-tide flooding. *Nature Climate Change*, *11*(7), 584–590. https://doi.org/10.1038/s41558-021-01077-8

Thompson, P. R., Widlansky, M. J., Merrifield, M. A., Becker, J. M., & Marra, J. J. (2019). A statistical model for frequency of coastal flooding in Honolulu, Hawaii, during the 21st century. *Journal of Geophysical Research: Oceans*, *124*(4), 2787–2802. https://doi.org/10.1029/2018jc014741

Vitousek, S., Barnard, P. L., Fletcher, C. H., Frazer, N., Erikson, L., & Storlazzi, C. D. (2017). Doubling of coastal flooding frequency within decades due to sea-level rise. *Scientific Reports*, *7*(1), 1399. https://doi.org/10.1038/s41598-017-01362-7

Vousdoukas, M. I., Mentaschi, L., Voukouvalas, E., Verlaan, M., & Feyen, L. (2017). Extreme sea levels on the rise along Europe's coasts. *Earth's Future*, *5*(3), 304–323. https://doi.org/10.1002/2016EF000505

Wahl, T., Jain, S., Bender, J., Meyers, S. D., & Luther, M. E. (2015). Increasing risk of compound flooding from storm surge and rainfall for major US cities. *Nature Climate Change*, *5*(12), 1093–1097. https://doi.org/10.1038/nclimate2736

Wang, J., Gao, W., Xu, S., & Yu, L. (2012). Evaluation of the combined risk of sea level rise, land subsidence, and storm surges on the coastal areas of Shanghai, China. *Climatic Change*, *115*(3), 537–558. https://doi.org/10.1007/s10584-012-0468-7

Wang, K., Yang, Y., Reniers, G., & Huang, Q. (2021). A study into the spatiotemporal distribution of typhoon storm surge disasters in China. *Natural Hazards*, *108*(1), 1237–1256. https://doi.org/10.1007/s11069-021-04730-9

Wu, S., Feng, A., Gao, J., Chen, M., Li, Y., & Wang, L. (2017). Shortening the recurrence periods of extreme water levels under future sea-level rise. *Stochastic Environmental Research and Risk Assessment*, *31*(10), 2573–2584. https://doi.org/10.1007/s00477-016-1327-2

Xu, H., Xu, K., Lian, J., & Ma, C. (2019). Compound effects of rainfall and storm tides on coastal flooding risk. *Stochastic Environmental Research and Risk Assessment*, *33*(7), 1249–1261. https://doi.org/10.1007/s00477-019-01695-x

Zhang, W., Cao, Y., Zhu, Y., Zheng, J., Ji, X., Xu, Y., et al. (2018). Unravelling the causes of tidal asymmetry in deltas. *Journal of Hydrology*, *564*, 588–604. https://doi.org/10.1016/j.jhydrol.2018.07.023